Available online at www.sciencedirect.com
ScienceDirect
International Journal of Heat and Mass Transfer 51 (2008) 176–185
International Journal of HEAT and MASS TRANSFER
www.elsevier.com/locate/ijhmt

Estimation of inhomogeneous zeta potential in the electroosmotic flow by means of mode reduction

H.M. Park *, S.M. Hong, J.S. Lee

Department of Chemical and Biomolecular Engineering, Sogang University, Seoul, South Korea

Received 19 November 2006; received in revised form 10 April 2007
Available online 19 June 2007

Abstract

A reduced-order model is derived for electroosmotic flows in a microchannel of nonuniform cross-section. The model is constructed based on the Karhunen–Loève Galerkin (KLG) procedure which can reduce nonlinear partial differential equations to sets of minimal number of ordinary differential equations. The reduced-order model of the present investigation is carefully constructed such that it is not necessary to re-evaluate any coefficient of the model even though the inhomogeneous zeta potential $\zeta(x)$ and the dielectric constant ε vary. This feature reduces the computational time greatly when employed in the estimation and control of electroosmotic flows, where repeated solution of governing equations is required. Using the present reduced-order model, a practical method is devised to estimate inhomogeneous zeta potential $\zeta(x)$ from velocity measurements of the electroosmotic flow in the microchannel. The proposed method is found to estimate $\zeta(x)$ with reasonable accuracy even using noisy velocity measurements.

1. Introduction

Microfluidic devices and systems find applications in inkjet printing, blood analysis, biochemical detection, chemical synthesis, drug screening and delivery, protein analysis, DNA sequencing and so on [1–3]. In these devices and systems the target chemical species are delivered by activating electroosmotic flow. Electroosmotic flow is generated when an electric field is imposed through an ionic solution parallel to the charged surfaces of a capillary [4]. The movement of ions in the electric double layer, caused by the external electric field, acts as a driving force of the electroosmotic flows.

Electroosmotic flows depend on the zeta potential, which varies with solution pH, ionic strength and solute molecules adsorbed into the walls. Electrochemical reactions, which must occur at electrodes in order to impose an electric field in solution, incurs metallic ion injection, water electrolysis and the variation of pH. These adverse effects may influence the zeta potential distribution along the channel wall. Since the zeta potential ζ is a crucial factor influencing the electroosmotic flows, it is imperative to determine accurate values of ζ before guaranteeing a secure operation of the system. Inhomogeneous zeta potential occurs due to several reasons. The surface heterogeneity is introduced intentionally by chemical surface modification to induce vortex or secondary flow. Or unwanted adhesion of DNA or protein to the channel wall causes the nonuniform zeta potential along the channel in various lab-chips. Considering the fact that ζ distribution may vary during the operation of the devices it is necessary to perform a real-time estimation of $\zeta(x)$ for the control of such devices. Because estimation and control of a system require repeated computation of governing equations, one of the most important prerequisites for the estimation and control of these microfluidic devices is appropriate dynamic modeling of the system which allows real-time simulation as well as accurate prediction. In the present investigation we employ the Karhunen–Loève Galerkin procedure (KLG procedure) to derive a reduced-order model for electroosmotic flows in microchannels. The Karhunen–Loève Galerkin procedure is a type of Galerkin methods, which employs the empirical eigenfunctions of the Karhunen–Loève decomposition as

* Corresponding author. Tel.: +82 2 705 8482.
E-mail address: hmpark@sogang.ac.kr (H.M. Park).

0017-9310/$ - see front matter © 2007 Elsevier Ltd. All rights reserved.
doi:10.1016/j.ijheatmasstransfer.2007.04.016

basis functions [5–8]. Employing the empirical eigenfunction of the Karhunen–Loève decomposition as basis functions of a Galerkin procedure, one can reduce the given partial differential equations to a minimal set of ordinary differential equations. Then, sophisticated control and estimation techniques can be applied rigorously without undue mathematical and computational complexities to this small set of ordinary differential equations [9,10]. Recently the KLG procedure has been applied successfully to the optimal feedback control of the Rayleigh–Bénard convection whose governing equation consist of the Navier–Stokes equation and the heat convection equation [11,12].

However, there are two significant obstacles to the straightforward application of the KLG procedure to the electroomotic flows. One obstacle is the steep profiles of electric potential and velocity near the walls. The KLG procedure usually yields satisfactory results when applied to the modelling of fields with smooth variation. But fields with steep gradient are not easily resolved by empirical eigenfunction. The other obstacle is the exponential dependence of the charge density on the electric potential. The body force term of the Navier–Stokes equation for eletroosmotic flows consists of net charge density multiplied by the electric potential gradient. The governing equation for the electric potential is the Poisson–Boltzmann equation [4], which also has the exponential of electric potential as a source term. Therefore, the electric potential field must be reconstructed using the relevant empirical eigenfunctions before performing the projection of the exponential terms into the basis space when simulating the flow field using a Galerkin method. This point will be expounded further in a later section. If the electric potential changes due to the variation of the zeta potential or the dielectric constant, the repeated reconstruction of the electric potential and evaluation of the inner product cause significant consumption of computer time especially in the parameter estimation procedure or modern control scheme. In the present investigation, these difficulties are circumvented by representing the electric potential as a sum of the boundary function, which is the analytic solution of one-dimensional Poisson–Boltzmann equation, and a perturbation function.

To demonstrate the efficiency and accuracy of the derived reduced-order model, it is applied to estimate the spatially inhomogeneous zeta potential using velocity measurements of electroosmotic flow in a microchannel. This is an inverse problem of finding the cause from a known result. The solution of inverse problems is not straightforward due to their ill-posedness. Namely, small perturbation in the observed function may result in large changes in the corresponding solution [13]. One powerful method of solving inverse problems, which alleviates the difficulties associated with the ill-posed nature, is to convert them into minimization problems of a performance function using the conjugate gradient method [14]. The performance function is usually posed by the sum of square residuals between calculated and observed velocity at measurement locations. While performing the conjugate gradient iteration to minimize the performance function, it is necessary to solve governing equations repeatedly. Thus, the employment of the reduced-order model instead of the partial differential functions will facillitate the estimation procedure significantly.

2. The Karhunen–Loève decomposition

As a means of explaining the Karhunen–Loève decomposition we select N arbitrary irregularly shaped functions with $n = 1, 2, \ldots, N$. From now on, we call the irregular shapes of these functions $\{v_n\}$ 'snapshots'. The issue is how to obtain the most typical or characteristic structure $\phi(x)$ among these snapshots $\{v_n\}$. It can be shown that the required function $\phi(x)$ can be found by solving the following eigenvalue problem of the integral equation (1) [15]:

$$\int_{\Omega} K(\mathbf{x}, \mathbf{x}')\phi(\mathbf{x}')\,\mathrm{d}x' = \lambda\phi(\mathbf{x}), \tag{1}$$

where $K(\mathbf{x}, \mathbf{x}')$ is the two point correlation function defined as

$$K(\mathbf{x}, \mathbf{x}') = \langle v_n(\mathbf{x})v_n(\mathbf{x}')\rangle = \frac{1}{N}\sum_{n=1}^{N} v_n(\mathbf{x})v_n^T(\mathbf{x}'). \tag{2}$$

Usually this kind of integral equation can be solved by means of Schmidt–Hilbert technique [16].

Let us express the eigenvalues, $\lambda_1 > \lambda_2 > \cdots > \lambda_N$ and the corresponding eigenfunctions $\phi_1, \phi_2, \ldots, \phi_N$ in the order of magnitude of eigenvalues. The eigenfunction ϕ_1 corresponding to the largest eigenvalue λ_1 is the most typical structure of the member of the snapshots $\{v_n\}$ and the eigenfunction ϕ_2 with the next largest eigenvalue λ_2 is the next typical structure, and so forth. These empirical eigenfunctions $\{\phi_n\}$ can represent the system in the most efficient way, and when employed as the basis functions of a Galerkin method the system can be represented with the minimum degree of freedom [17,18].

3. The system and governing equations

We consider a simple electrolyte that dissociates into two equally charged ions of valence z and $-z$. The electric potential in the electric double layer, induced by these ions, is governed by the Poisson–Boltzmann equation [4].

The following dimensionless variables are defined:

$$\begin{aligned}
&\mathbf{x}^* = \frac{\mathbf{x}}{L}, \quad \psi^* = \frac{\psi}{\zeta_0}, \quad \mathbf{v}^* = \frac{\mathbf{v}}{U}, \quad p^* = \frac{p}{\rho_{\mathrm{f}}U^2},\\
&t^* = \frac{t}{L/U}, \quad \phi^* = \frac{\phi}{\zeta_0},\\
&\omega = \frac{1}{\kappa} = \sqrt{\frac{8\pi n_0 e^2 z^2}{\varepsilon_0\varepsilon k_{\mathrm{B}}T}}, \quad \alpha = \frac{ez\zeta_0}{k_{\mathrm{B}}T}, \quad \beta = \frac{(wL)^2}{\alpha} = \frac{L^2 8\pi n_0 ez}{\varepsilon_0\varepsilon\zeta_0},\\
&\delta = \frac{zen_0\zeta_0}{\rho_{\mathrm{f}}U^2}, \quad Re = \frac{\rho LU}{\mu},
\end{aligned} \tag{3}$$

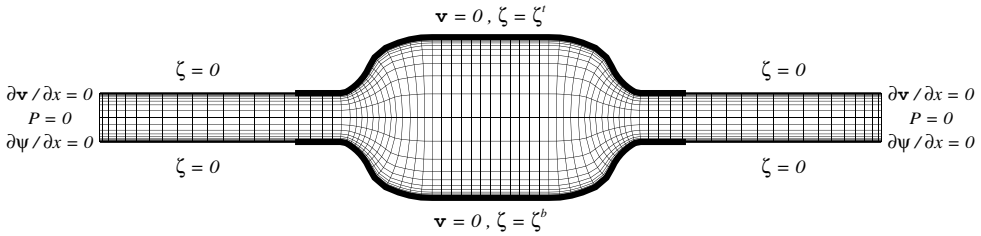

Fig. 1. Boundary conditions for the electroosmotic flow and the grid system (80 × 50) adopted in the numerical solution.

where ψ is the electric potential induced by ions, ϕ is the external potential, n_0 is the bulk ionic concentration, e is elementary charge, ε_0 is the permittivity of vacuum, ε is the dielectric constant, k_B is the Boltzmann constant, T is temperature, L is the width of channel, ζ_0 is the zeta potential at a reference position, U is the characteristic velocity, κ is the Debye length and Re is the Reynolds number. The surface potential is assumed to be the same as the zeta potential [19]. Then governing equations of the electroosmotic flow may be written using these dimensionless variables as follows:

$$\frac{\partial \mathbf{v}^*}{\partial t^*} + \mathbf{v}^* \cdot \nabla^* \mathbf{v}^* = -\nabla^* p^* + \frac{1}{Re}\nabla^{*2}\mathbf{v}^* + 2\delta \sinh(\alpha\psi^*)\nabla^*\phi^*, \tag{4}$$

$$\nabla \cdot \mathbf{v}^* = 0, \tag{5}$$

$$\nabla^{*2}\psi^* = \beta \sinh(\alpha\psi^*). \tag{6}$$

From now on we use Eqs. (4)–(6) as the set of governing equations after deleting the asterisks for the sake of brevity. The relevant boundary conditions for these equations are specified in Fig. 1 for the case of a two-dimensional channel with nonuniform cross-sectional area. The governing equations (4) and (5) are solved using the SIMPLE algorithm [20–23] after transforming the physical domain (x, y) into a square computational domain (X, Y). The numerical solution of Eq. (6) requires the Newton–Raphson iteration. The grid system employed in the numerical solution is depicted also in Fig. 1. The grids are massively clustered near the channel walls to resolve the thin electric double layer. The number of grids in the vertical direction is 50, and a further increase of grids does not change the numerical results.

4. The Karhunen–Loève Galerkin procedure for the electroosmotic flows

The Karhunen–Loève Galerkin (KLG) procedure consists of the following three basic steps: preparation of various electric potential fields and velocity fields called the snapshots, extraction of empirical eigenfunctions from these fields, construction of the reduced-order model using empirical eigenfunctions [5,6]. However, the application of KLG procedure to the electroosmotic flow is not easy due to the steep gradient of the electric potential near the channel walls. Usually, the KLG procedure yields accurate results for smooth fields. On the contrary, the extraction of empirical eigenfunctions from fields with rapid spatial variation, such as shock waves, is not easy and the accuracy of the KLG procedure for such systems is not satisfactory. The ψ field can be converted to a smooth field as follows. The electric potential field, governed by Eq. (6), varies rapidly from $\psi = \zeta$ (zeta potential value) at the wall to $\psi = 0$ at the outer edge of the electric double layer whose thickness is determined by the Debye length κ defined in Eq. (3). The Debye length κ shrinks down as the bulk ionic concentration n_0 increases, which is equivalent to the increased values of the dimensionless groups α and β defined in Eq. (3). Typical parameter values for electroosmotic flows in microchannels are as follows:

$$\begin{aligned} &e = 1.602 \times 10^{-19}\ \mathrm{C}, \quad z = 1, \quad \zeta_0 = 100\ \mathrm{mV}, \\ &k_B = 1.381 \times 10^{-23}\ \mathrm{J/K}, \quad T = 298\ \mathrm{K}, \quad L = 10^{-4}\ \mathrm{m}, \\ &\varepsilon = 78.5, \quad \varepsilon_0 = 8.85 \times 10^{-12}\ \mathrm{C^2/N\,m^2}, \\ &n_0 = 10^{-6}\ \mathrm{mol/l}, \quad Re = 0.1. \end{aligned} \tag{7}$$

For the above parameter values, we find

$$\alpha = 3.89, \quad \beta = 3.593 \times 10^5, \quad \delta = 2.85 \times 10^{-5}\alpha^2\beta \tag{8}$$

and the Debye length κ, which is given by $\frac{L}{\sqrt{\alpha\beta}}$, is less than one ten-thousandth of the channel width. The electric potential variation is thus mostly one dimensional in the normal direction and the steamwise variation is not so much significant. Exploiting this, we decompose the electric potential field ψ into the following two parts:

$$\psi = \psi^h + \pi, \tag{9}$$

where π is determined by the one-dimensional Poisson–Boltzmann equation.

$$\frac{\partial^2 \pi}{\partial \eta^2} = \beta \sinh(\alpha\pi), \tag{10}$$

where η is the scaled normal distance from the wall. The relevant boundary conditions for π are

$$\eta = 0, \quad \pi = \zeta; \quad \eta = \infty, \quad \pi = 0, \tag{11}$$

where ζ is the dimensionless zeta potential normalized with respect to ζ_0. The above function π approximates the normal variation of ψ and the deviation from the exact solution is given by the perturbation function ψ^h, which is small and has smooth variation for most values of α and

β. The exact solution of Eqs. (10) and (11) is derived in Hunter [19] and reproduced below.

$$\pi(X,\eta) = \frac{2}{\alpha}\ln\left[\frac{1+e^{-\sqrt{\alpha\beta}\eta}\tanh\left(\frac{\alpha}{4}\zeta\right)}{1-e^{-\sqrt{\alpha\beta}\eta}\tanh\left(\frac{\alpha}{4}\zeta\right)}\right]. \tag{12}$$

This function approaches to zero rapidly as η increases for practical range of α and β. For the later convenience, we call π the boundary function. Substituting Eq. (9) into Eq. (6) and expanding $e^{\alpha\psi^h}$ and $e^{-\alpha\psi^h}$ up to the first order in $\alpha\psi^h$ using the Taylor series, Eq. (6) becomes the following linear equation for the perturbation function ψ^h.

$$\nabla^2\psi^h = \frac{\alpha\beta}{2}[e^{\alpha\pi}+e^{-\alpha\pi}]\psi^h + \frac{\beta}{2}[e^{\alpha\pi}-e^{-\alpha\pi}] - \nabla^2\pi. \tag{13}$$

Once π is obtained using Eq. (12), for given values of α, β and ζ, Eq. (13) is solved very easily without the necessity of Newton–Raphson iteration since it is a linear equation for a small and smooth field ψ^h. Extraction of empirical eigenfunctions for ψ^h is also easy since ψ^h has a smooth spatial variation. Another important fact to be the mentioned is that there is no exponential dependance on ψ^h in Eq. (13) contrary to the ψ field in Eq. (6). If we are to solve Eq. (6) for ψ using a Galerkin method, the ψ field must be reconstructed from the basis functions to perform the Galerkin projection of the exponential term. This will delay the speed of numerical computation significantly. On the contrary, the numerical solution of Eq. (13) using a Galerkin method does not require the reconstruction of ψ^h once the boundary function π has been evaluated.

Now we proceed to the steps of KLG for the electroosmotic flows in microchannels. The final objective is to derive a reduced-order model that simulates the eletroosmotic flows in a microchannel with arbitrary distribution of ζ at the upper wall. Moreover the reduced-order model is to be constructed such that the reconstruction of ψ or $\mathbf{v}$ is never required even though the ζ distribution varies. This is one of the most important requirements of efficient reduced-order model, since the reduced-order model must be solved repeatedly for various values of ζ when performing parameter estimation needed in real-time control.

4.1. The KLG procedure for the boundary function π

Although the boundary function π can be evaluated easily using Eq. (12) for a given set of (α,β,ζ), it is necessary to extract empirical eigenfunctions for π, $e^{\alpha\pi}$ and $e^{-\alpha\pi}$ to avoid the reevaluation of the inner product integrals in the KLG procedure. For this propose, we introduce the so-called masking functions $h^a(x,y)$, $h^b(x,y)$ and $h^c(x,y)$ governed by

$$\nabla^2 h^a = 0; \quad \nabla^2 h^b = 0; \quad \nabla^2 h^c = 0. \tag{14}$$

The boundary conditions for h^a, h^b and h^c are shown in Fig. 2. The boundary conditions for h^a are such that $h^a = 1.0$ at the upper boundary and h^a is identically zero for points whose distance from the upper boundary is longer than ℓ, which is arbitrary but a reasonable choice is the

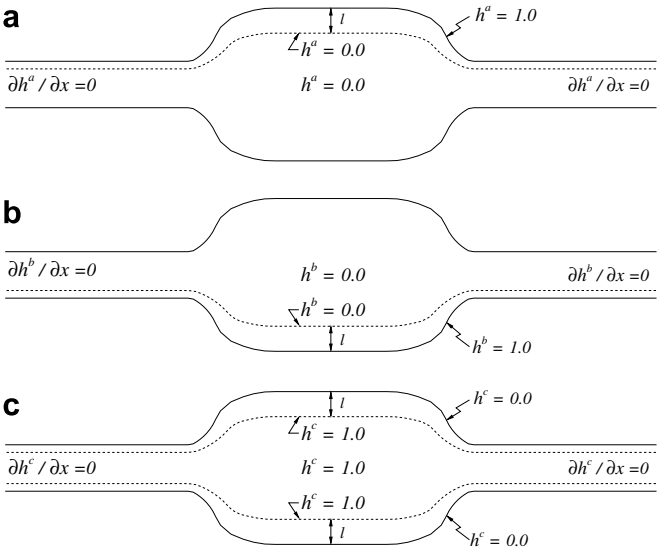

Fig. 2. Boundary conditions for the masking functions h^a, h^b and h^c.

Debye length. The masking function h^b has similar boundary conditions, the only difference being $h^b = 1.0$ at the lower boundary. The value of h^c is identically 1 outside the electric double layer (EDL), and has values less than one inside the EDL and becomes zero at the walls. Then the reference fields for π, $e^{\alpha\pi}$, $e^{-\alpha\pi}$, which are needed to make the snapshots homogeneous [5,6], are defined by

$$\pi^r = \zeta^t h^a + \zeta^b h^b; \quad e^{\alpha\pi^r} = e^{\alpha\zeta^t}h^a + e^{\alpha\zeta^b}h^b + h^c;$$
$$e^{-\alpha\pi^r} = e^{-\alpha\zeta^t}h^a + e^{-\alpha\zeta^b}h^b + h^c, \tag{15}$$

where ζ^t and ζ^b are the zeta potential at the upper and lower walls as shown in Fig. 1. These reference fields π^r, $e^{\alpha\pi^r}$ and $e^{-\alpha\pi^r}$ have the same boundary values as π, $e^{\alpha\pi}$ and $e^{-\alpha\pi}$, respectively. The variation of the zeta potential in the streamwise direction can be taken care of by introducing a set of linear basis functions depicted in Fig. 3. The linear basis function $b_p(X)$ is defined such that $b_i(X_p) = \delta_{p_i}$ and resembles a hat function. Then

$$\zeta^t = \sum_{p=1}^{M_x}\zeta_p^t b_x(X); \quad e^{\alpha\zeta^t} \simeq \sum_{p=1}^{M_x} e^{\alpha\zeta_p^t} b_p(X);$$
$$e^{-\alpha\zeta^t} \simeq \sum_{p=1}^{M_x} e^{-\alpha\zeta_p^t} b_p(X) \tag{16}$$

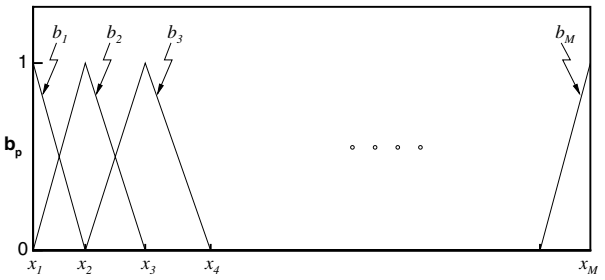

Fig. 3. Definition of linear basis functions.

and the reference fields are represented by

$$\pi^r = \sum_{p=1}^{M_x} \zeta_p^t h^a b_p(X) + \sum_{p=1}^{M_x} \zeta_p^b h^b b_p(X), \tag{17}$$

$$\mathrm{e}^{\alpha\pi^r} = \sum_{p=1}^{M_x} \mathrm{e}^{\alpha\zeta_p^t} h^a b_p(X) + \sum_{p=1}^{M_x} \mathrm{e}^{\alpha\zeta_p^b} h^b b_p(X) + h_c, \tag{18}$$

$$\mathrm{e}^{-\alpha\pi^r} = \sum_{p=1}^{M_x} \mathrm{e}^{-\alpha\zeta_p^t} h^a b_p(X) + \sum_{p=1}^{M_x} \mathrm{e}^{-\alpha\zeta_p^b} h^b b_p(X) + h_c, \tag{19}$$

where M_x is the number of linear basis functions employed, which is the same as the grid numbers in the streamwise direction. To prepare snapshots for the boundary function π that cover arbitrary profile of the zeta potential at the upper wall, we evaluate π using Eq. (12) for $\zeta = 0$ except at one grid point at the upper wall where $\zeta = 0.5$ or 1.0 or 1.5. We repeat this procedure for every grid points of the upper wall, when $\alpha = 3.89$ and $\beta = 3.593 \times 10^5$. Then the relevant homogeneous snapshots are given by

$$\hat{\pi} = \pi - \pi^r; \quad \hat{\mathrm{e}}^{\alpha\pi} = \mathrm{e}^{\alpha\pi} - \mathrm{e}^{\alpha\pi^r}; \quad \hat{\mathrm{e}}^{-\alpha\pi} = \mathrm{e}^{-\alpha\pi} - \mathrm{e}^{-\alpha\pi^r}. \tag{20}$$

The Karhunen–Loève decomposition [5] is applied to these homogenous snapshots $\hat{\pi}, \hat{\mathrm{e}}^{\alpha\pi}$, and $\hat{\mathrm{e}}^{-\alpha\pi}$ to find the corresponding empirical eigenfunctions $\{\varphi^m\}$, $\{\theta^{2m}\}$, and $\{\theta^{1m}\}$, respectively. Using these sets of empirical eigenfunctions π, $\mathrm{e}^{\alpha\pi}$, and $\mathrm{e}^{-\alpha\pi}$ may be represented as

$$\pi = \pi^r + \sum_{m=1}^{L} d_m \varphi^m; \quad \mathrm{e}^{\alpha\pi} = \mathrm{e}^{\alpha\pi^r} + \sum_{m=1}^{L} c_m \theta_m^2;$$

$$\mathrm{e}^{-\alpha\pi} = \mathrm{e}^{-\alpha\pi^r} + \sum_{m=1}^{L} b_m \theta_m^1. \tag{21}$$

4.2. The KLG procedure for the electric potential ψ

The snapshots for the electric potential ψ are obtained in a similar way. Namely, we solve Eq. (6) for $\zeta = 0$ except at one grid point at the upper wall where $\zeta = 0.5$ or 1.0 or 1.5. We repeat this procedure for every grid point of the upper wall, when $\alpha = 3.89$ and $\beta = 3.593 \times 10^5$. The homogeneous snapshots ψ^h are obtained by Eq. (9). Applying the Karhunen–Loève decomposition to the snapshots $\{\psi^h\}$, the empirical eigenfunctions $\{\Theta^m\}$ are obtained. Then we may represent ψ^h as

$$\psi^h = \sum_{m=1}^{N} e_m \Theta^m, \tag{22}$$

where N is the number of empirical eigenfunctions employed. We may confirm the accuracy of these empirical eigenfunctions $\{\varphi^m\}$, $\{\theta_m^2\}$, $\{\theta_m^1\}$, and $\{\Theta^m\}$ by comparing π, $\mathrm{e}^{\alpha\pi}$ and $\mathrm{e}^{-\alpha\pi}$ obtained by Eq. (21) with those obtained by Eq. (12) and ψ from Eq. (22) with that from Eq. (6), for an arbitrary profile of ζ shown in Fig. 4a. The reconstruction error is defined for a field ϕ as

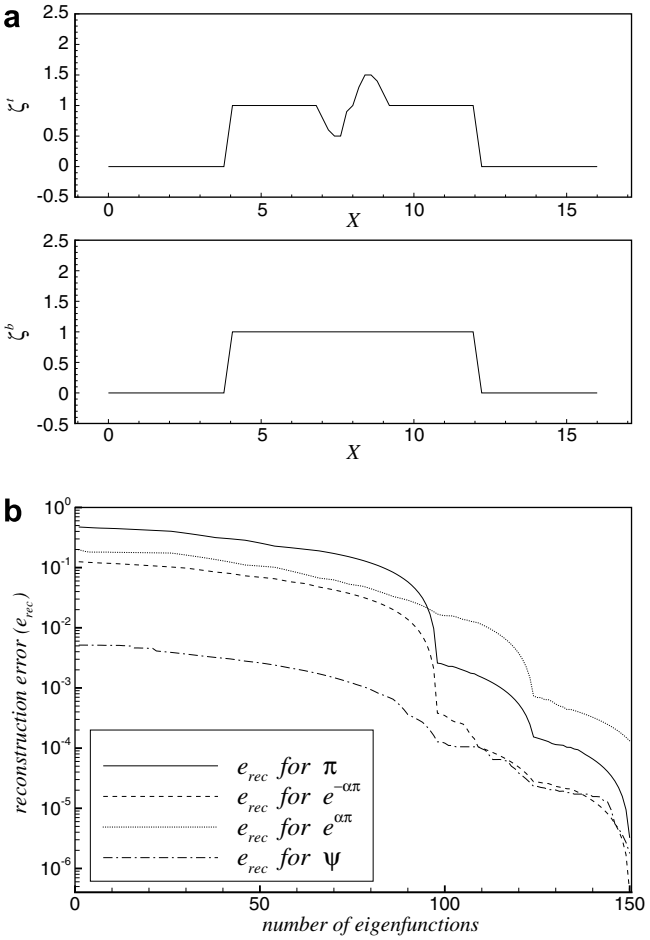

Fig. 4. Reconstruction errors of π, $\mathrm{e}^{\alpha\pi}$, $\mathrm{e}^{-\alpha\pi}$ and ψ versus the number of eigenfunctions.

$$\mathrm{e}_{\mathrm{rec}} \equiv \frac{\|\phi_{\mathrm{rec}} - \phi_{\mathrm{ext}}\|_{L2}}{\|\phi_{\mathrm{ext}}\|_{L2}}, \tag{23}$$

where ϕ_{ext} is the field obtained by Eq. (12) or (6) and ϕ_{rec} is the corresponding field obtained by Eq. (21) or (22). Fig. 4b shows the reconstruction errors of π, $\mathrm{e}^{\alpha\pi}$, $\mathrm{e}^{-\alpha\pi}$ and ψ with respect to the number of corresponding eigenfunctions. It is show that sufficient accuracy is attained if L is larger than 150 and N is larger than 70.

Substituting Eq. (22) into Eq. (13) and applying the Galerkin principle which enforces the residual to be orthogonal to each of the basis functions Θ^m, Eq. (13) is converted to the following algebraic equations for e_m:

$$-\sum_{m=1}^{N} e_m \int_\Omega (\nabla^2 \Theta^m)\Theta^P \,\mathrm{d}\Omega + \sum_{m=1}^{N} e_m \frac{\alpha\beta}{2} \int [\mathrm{e}^{\alpha\pi} + \mathrm{e}^{-\alpha\pi}]\Theta^m \Theta^P \,\mathrm{d}\Omega$$
$$= -\frac{\beta}{2} \int [\mathrm{e}^{\alpha\pi} - \mathrm{e}^{-\alpha\pi}]\Theta^P \,\mathrm{d}\Omega + \int_\Omega (\nabla^2 \pi)\Theta^p \,\mathrm{d}\Omega$$
$$(P = 1, 2, \ldots, N). \tag{24}$$

Substituting Eqs. (17)–(19) into Eq. (24), the final form of the reduced-order model for ψ^h is derived.

$$\sum_{m=1}^{N} C^{\psi}_{pm} e_m = D^{\psi}_p \quad (p = 1, 2, \ldots, N), \tag{25}$$

where C^{ψ}_{pm} and D^{ψ}_p depend upon α, β, ζ^t_ℓ and ζ^b_ℓ ($\ell = 1, 2, \ldots, M_x$)

$$C^{\psi}_{pm} \equiv N^1_{pm} + \frac{\alpha\beta}{2}\sum_{\ell=1}^{M_x}(e^{\alpha\zeta^t_\ell} + e^{-\alpha\zeta^t_\ell})N^{2,\ell}_{pm} + \frac{\alpha\beta}{2}\sum_{\ell=1}^{M_x}(e^{\alpha\zeta^b_\ell} + e^{-\alpha\zeta^b_\ell})N^{3,\ell}_{pm} + \frac{\alpha\beta}{2}N^4_{pm} + \frac{\alpha\beta}{2}\sum_{s=1}^{L} C_s H^1_{pms} + \frac{\alpha\beta}{2}\sum_{s=1}^{L} b_s H^2_{pms}, \tag{26}$$

$$D^{\psi}_p \equiv -\frac{\beta}{2}\sum_{\ell=1}^{M_x}(e^{\alpha\zeta^t_\ell} - e^{-\alpha\zeta^t_\ell})M^{1,\ell}_p - \frac{\beta}{2}\sum_{\ell=1}^{M_x}(e^{\alpha\zeta^b_\ell} - e^{-\alpha\zeta^b_\ell})M^{2,\ell}_p - \frac{\beta}{2}\sum_{s=1}^{L} C_s N^7_{ps} + \frac{\beta}{2}\sum_{s=1}^{L} b_s N^8_{ps} + \sum_{s=1}^{L} d_s N^9_{ps} + \sum_{\ell=1}^{M_x}\zeta^t_\ell M^{3,\ell}_p + \sum_{\ell=1}^{M_x}\zeta^b_\ell M^{4,\ell}_p. \tag{27}$$

The matrix coefficients in Eqs. (26) and (27) are defined by

$$N^1_{pm} = -\int_\Omega (\nabla^2\Theta^m)\Theta^p \,d\Omega, \quad N^{2,\ell}_{pm} = \int_\Omega h^a \hat{b}_\ell(x)\Theta^m\Theta^p \,d\Omega,$$
$$N^{3,\ell}_{pm} = \int_\Omega h^b \hat{b}_\ell(x)\Theta^m\Theta^p \,d\Omega, \quad N^4_{pm} = \int_\Omega 2h^c\Theta^m\Theta^p \,d\Omega,$$
$$H^1_{pms} = \int_\Omega \theta^{2s}\Theta^m\Theta^p \,d\Omega, \quad H^2_{pms} = \int_\Omega \theta^{1s}\Theta^m\Theta^p \,d\Omega,$$
$$M^{1,\ell}_p = \int_\Omega h^a \hat{b}_p(x)\Theta^p \,d\Omega, \quad M^{2,\ell}_p = \int_\Omega h^b \hat{b}_p(x)\Theta^p \,d\Omega,$$
$$M^{3,\ell}_p = \int_\Omega \Theta^p\nabla^2(h^a\hat{b}_\ell) \,d\Omega, \quad M^{4,\ell}_p = \int_\Omega \Theta^p\nabla^2(h^b\hat{b}_\ell) \,d\Omega,$$
$$N^7_{ps} = \int_\Omega \theta^{2s}\Theta^p \,d\Omega, \quad N^8_{ps} = \int_\Omega \theta^{1s}\Theta^p \,d\Omega,$$
$$N^9_{ps} = \int_\Omega \Theta^p\nabla^2\varphi^s \,d\Omega. \tag{28}$$

Eq. (25) is a set of linear algebraic equations whose solution $\{e_m\}$ can be obtained by a simple matrix inversion. The novelty of Eqs. (25)–(27) is the fact that it is not necessary to reevaluate the integrals defined in Eq. (28), which arise from the inner products of the Galerkin procedure, when α, β and ζ vary. If we had applied the KLG procedure to Eq. (6), the integrals of the inner product would have to be recalculated after constructing ψ from the corresponding empirical eigenfunctions whenever α, β and ζ change. Fig. 5 shows the comparison of the ψ fields from the numerical solution of Eq. (6) with that from the reduced-order model (25)–(27) at selected locations for an arbitrary profile of ζ when $L = 150$ and $N = 70$. It is shown that the two results coincide almost exactly. Further increase of the number of empirical eigenfunctions (L and N) did not improve the accuracy.

4.3. The KLG procedure for the velocity field

The procedure for the preparation of velocity snapshots depends on the objective of the reduced-order model. In

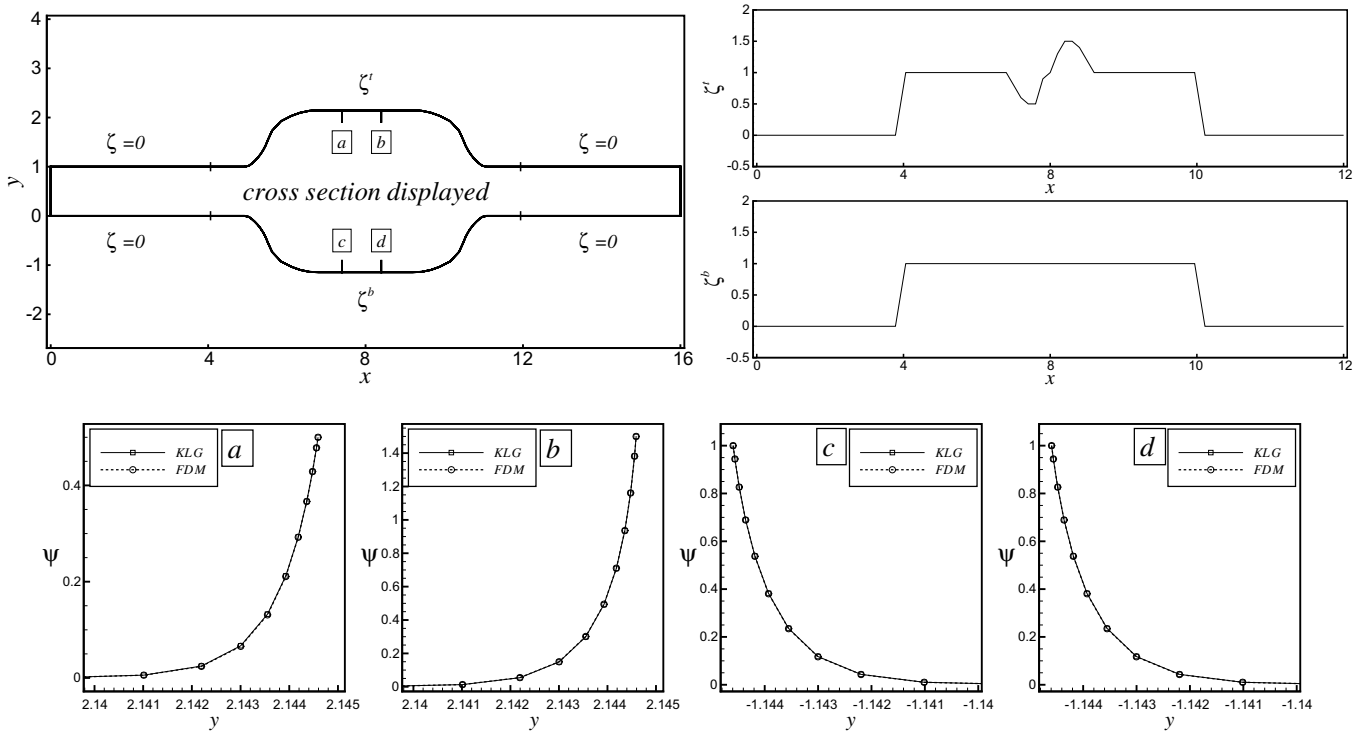

Fig. 5. Accuracy of the reduced-order model for the electric potential field ψ.

the present investigation, it is intended to simulate the electroosmotic flows when the external potential ϕ varies time periodically. The external potential ϕ is obtained as

$$\phi = \phi^r aLe \cos \omega t, \tag{29}$$

where Le is the length of the channel, $a = 100$ and $\omega = \pi/100$. It is assumed that ϕ and ϕ^r are governed by the Laplace equation

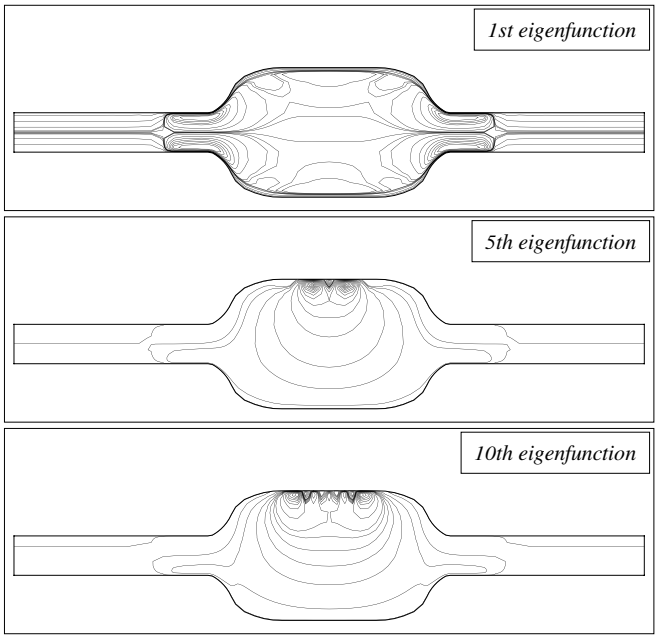

Fig. 6. Dominant empirical eigenfunctions for the velocity field, $\boldsymbol{\phi}_1$, $\boldsymbol{\phi}_5$ and $\boldsymbol{\phi}_{10}$.

$$\nabla^2 \phi = 0; \quad \nabla^2 \phi^r = 0. \tag{30}$$

The boundary conditions for ϕ and ϕ^r are such that $\phi = 0$ and $\phi^r = 0$ at the inlet, $\phi = a\cos\omega t$ and $\phi^r = 1$ at the outlet and the normal derivatives of ϕ and ϕ^r are zero at the wall. The velocity snapshots are obtained by solving Eqs. (4)–(6) with $\zeta = 1$ except at one grid point at the upper wall where $\zeta = 0.5$ or 1.0 or 1.5. From the resulting transient velocity fields we take 20 velocity snapshots. This procedure is repeated for every grid point of the upper wall. Applying the Karhunen–Loève decomposition to these velocity snapshots, the velocity empirical eigenfunctions $\{\boldsymbol{\phi}_m\} = \{(\phi^x_m, \phi^y_m)\}$ are obtained. Fig. 6 shows the first, the fifth and the 10th velocity eigenfunction. Then the velocity field can be represented by

$$\mathbf{v} = \sum_{m=1}^{M} a_m \boldsymbol{\phi}_m. \tag{31}$$

Substituting Eq. (31) into Eq. (4) and applying the Galerkin principle which requires the orthogonality of the residual to each of $\boldsymbol{\phi}_m$, one can derive a reduced-order model for the flow field. To remove the exponential function of ψ in Eq. (4), which causes repeated evaluation of inner product integral and reconstruction of ψ using empirical eigenfunctions whenever α, β or ζ varies, the following relation is exploited:

$$\sinh(\alpha\psi) = \frac{1}{\beta}\nabla^2\psi = \frac{1}{\beta}(\nabla^2\pi + \nabla^2\psi^h), \tag{32}$$

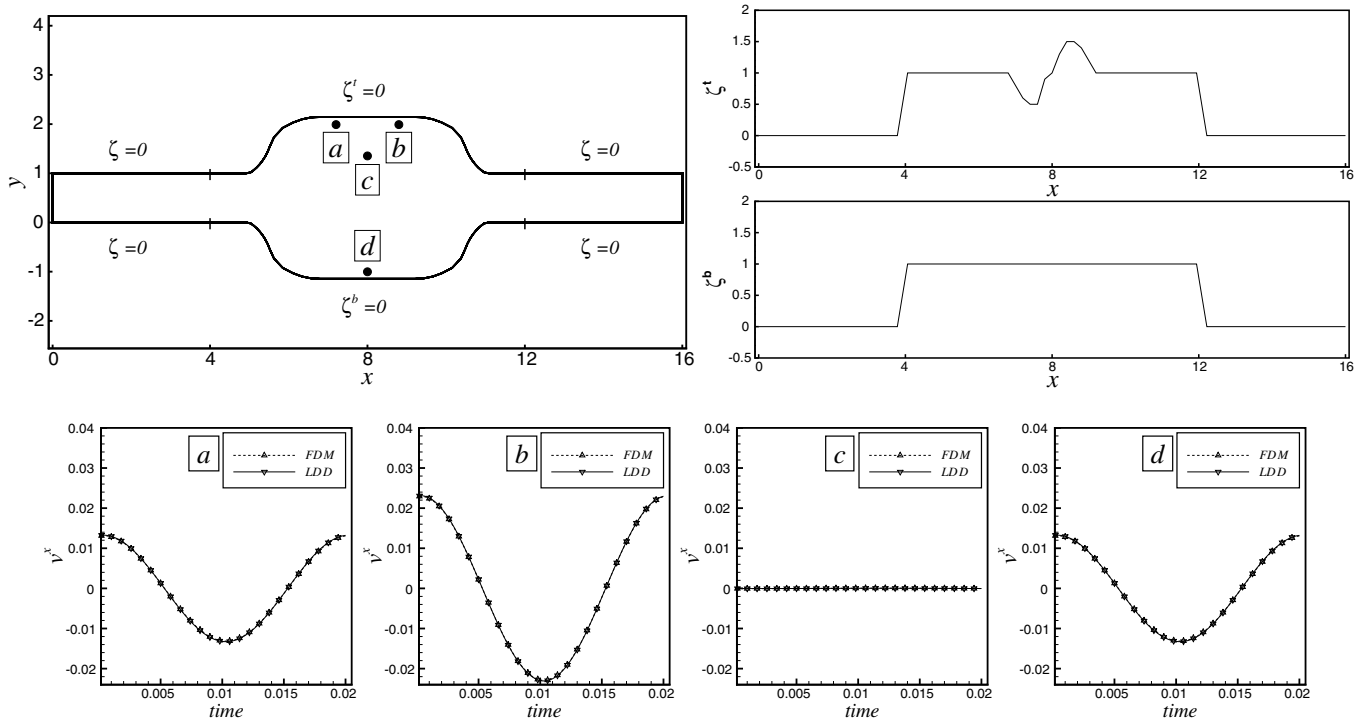

Fig. 7. Accuracy of reduced-order model for the flow field $\mathbf{v}$.

where π and ψ^h are to be represented by the relevant empirical eigenfunctions (cf. Eqs. (21) and (22)). The resulting reduced-order model for the flow field is

$$M_P \frac{\mathrm{d}a_P}{\mathrm{d}t} + \sum_{n=1}^{M}\sum_{\ell=1}^{M} Q_{Pn\ell} a_n a_\ell = -\frac{1}{Re}\sum_{n=1}^{M} H_{Pn} a_n + \frac{2\delta}{\beta}(aLe\cos\omega t) D_p^v \quad (P = 1, 2, \ldots, N), \tag{33}$$

where

$$D_p^v \equiv \sum_{s=1}^{L} d_s N_{Ps}^{11} + \sum_{m=1}^{N} e_m N_{Pm}^{12} + \sum_{\ell=1}^{M_x} \zeta_\ell^t M_P^{5\ell} + \sum_{\ell=1}^{M_x} \zeta_\ell^b M_P^{6\ell}. \tag{34}$$

The matrix coefficients in Eqs. (33) and (34) are defined by

$$M_P = \int_\Omega \boldsymbol{\phi}^{(P)} \cdot \boldsymbol{\phi}^{(P)}\,\mathrm{d}\Omega, \quad Q_{Pn\ell} = \int_\Omega \boldsymbol{\phi}^{(P)} \cdot (\boldsymbol{\phi}^{(n)} \cdot \nabla \boldsymbol{\phi}^{(\ell)})\,\mathrm{d}\Omega,$$

$$H_{Pn} = -\int_\Omega \boldsymbol{\phi}^{(P)} \cdot \nabla^2 \boldsymbol{\phi}^{(n)}\,\mathrm{d}\Omega, \quad N_{Ps}^{11} = \int_\Omega (\boldsymbol{\phi}^{(P)} \cdot \nabla \phi^r)(\nabla^2 \varphi^s)\,\mathrm{d}\Omega,$$

$$N_{Pm}^{12} = \int_\Omega (\boldsymbol{\phi}^{(P)} \cdot \nabla \phi^r)(\nabla^2 \Theta^m)\,\mathrm{d}\Omega,$$

$$M_P^{5,\ell} = \int_\Omega (\boldsymbol{\phi}^{(P)} \cdot \nabla \phi^r)\nabla^2 (h^a \hat{b}_\ell)\,\mathrm{d}\Omega,$$

$$M_P^{6,\ell} = \int_\Omega (\boldsymbol{\phi}^{(P)} \cdot \nabla \phi^r)\nabla^2 (h^b \hat{b}_\ell)\,\mathrm{d}\Omega. \tag{35}$$

The pressure gradient term in Eq. (4) is eliminated though integration by parts since the basis functions employed in the Galerkin procedure $\{\boldsymbol{\phi}_m\}$ are solenoidal.

Fig. 7 shows the accuracy of the reduced-order model, Eqs. (25) and (33) for the zeta potential profile shown in the same figure when $M = 15$. It is shows that the reduced-order model predicts the flow field accurately. Further increase of the number of velocity eigenfunctions employed in the reduced-order model, M, does not improve the accuracy appreciably. The reduced-order model constructed in this way can be employed to simulate the electroosmotic flow with arbitrary zeta potential profile at the upper wall.

5. Estimation of inhomogeneous zeta potential

While operating various lab-chips unwanted adhesion of DNA or protein to the microchannel wall causes nonuniform zeta potential along the channel wall, resulting in modification of flow pattern or flow rate. To revert to the prescribed flow pattern or flow rate, it is necessary to adjust the external electric potential. The implementation of this kind of control scheme requires the estimation of zeta potential profile modified by the adhesion of protein. In the present section, it shall be shown that the zeta potential profile can be estimated based on the velocity measurements accurately as well as efficiently if the reduced-order model developed in the previous sections is employed. This study may be regarded as a first step toward the application of modern control theory to various microfluidic devices. The velocity distribution in the microchannel may be measured using microparticle image velocity (μPIV) technique. Recent advances in microPIV allow measurements of velocity in the microchannel for a time resolution of 500 μs and a spatial resolution of 2.0 μm [24].

The following performance function is defined for the identification of $\zeta(x)$ using the velocity measurements.

$$J = \frac{1}{2}\int_{t_0}^{t_\mathrm{f}} \sum_{m=1}^{M_0} (\mathbf{v}(\zeta) - \mathbf{v}^*)_m^2\,\mathrm{d}t = \frac{1}{2}\int_{t_0}^{t_\mathrm{f}} \sum_{m=1}^{M_0} \left[\sum_{n=1}^{M} a_n(\zeta)\boldsymbol{\phi}_n - \mathbf{v}^*\right]_m^2, \tag{36}$$

where t_0 and t_f indicate the start and end of the measurement period, $\mathbf{v}^m(\zeta)$ is the model predicted velocity at the mth measurement location when $\zeta(x)$ is adopted as the zeta potential profile, $\mathbf{v}^{m^*}$ is the observed velocity at the same measurement location and M_0 is the total number of measurement locations. The $\zeta(x)$ that makes J zero is the correct profile of the zeta potential. Therefore, the estimation problem is tantamount to the minimization of J with respect to $\zeta(x)$ or with respect to ζ_p^t $(p = 1, 2, \ldots, M_x)$ (Eq. (16)) [13]. A powerful method of solving this kind of minimization problem is the conjugate gradient method [14]. The variation of J with respect to ζ_p^t is given by

$$\frac{\partial J}{\partial \zeta_p^t} = \sum_{m=1}^{M_0}\int_{t_0}^{t_\mathrm{f}} \left[\sum_{n=1}^{M} a_n(\zeta)\boldsymbol{\phi}_n - \mathbf{v}^*\right]_m \left[\sum_{r=1}^{M} \frac{\partial a_r}{\partial \zeta_p^t}\boldsymbol{\phi}_r\right]_m \mathrm{d}t \quad (p = 1, 2, \ldots, M_x). \tag{37}$$

The governing equations for the sensitivity functions, $\frac{\partial a_r}{\partial \zeta_p^t}$, are obtained by differentiating Eqs. (33), (34) and Eqs. (25)–(27) with respect to ζ_p^t. Define the vectors $\boldsymbol{\zeta}^t = (\zeta_1^t, \zeta_2^t, \ldots, \zeta_{M_x}^t)^\mathrm{T}$ and $\mathbf{a} = (a_1, a_2, \ldots, a_M)^\mathrm{T}$, and let Eq. (33) be denoted by $\mathbf{F} = 0$ and Eq. (25) by $\mathbf{G} = 0$, respectively. The governing equations for $\frac{\partial \mathbf{a}}{\partial \boldsymbol{\zeta}^t}$ are represented by

$$\frac{\partial \mathbf{F}}{\partial \boldsymbol{\zeta}^t} = 0, \quad \frac{\partial \mathbf{G}}{\partial \boldsymbol{\zeta}^t} = 0. \tag{38}$$

In Eq. (38) the $\frac{\partial e_m}{\partial \zeta^t}$ calculated from the solution of $\frac{\partial \mathbf{G}}{\partial \boldsymbol{\zeta}^t} = 0$ is used to solve $\frac{\partial \mathbf{F}}{\partial \boldsymbol{\zeta}^t} = 0$ for $\frac{\partial \mathbf{a}}{\partial \boldsymbol{\zeta}}$. The basic steps in the conjugate gradient method for the minimization of the performance function J may be described as follows [14]:

1. Assume $\boldsymbol{\zeta}^{t(0)}$ and calculate $\mathbf{a}$ and $\frac{\partial \mathbf{a}}{\partial \boldsymbol{\zeta}^t}$ using governing equations, (33), (34) and (25)–(27), and sensitivity equations (38).
2. Determine the conjugate direction at the ith iteration step $\mathbf{d}^{(i)}$ using

$$\mathbf{d}^{(i)} = -\frac{\partial J}{\partial \boldsymbol{\zeta}^{t(i)}} + \varphi \mathbf{d}^{(i-1)} \quad (i \geqslant 1), \tag{39}$$

where

$$\varphi \equiv \frac{\sum_{p=1}^{M_x}\left[\left(\frac{\partial J}{\partial \zeta_p^t}\right)^{(i)}\right]^2}{\sum_{p=1}^{M_x}\left[\left(\frac{\partial J}{\partial \zeta_p^t}\right)^{(i-1)}\right]^2} \quad (i \geqslant 1);\ \varphi \equiv 0\ (i=0). \tag{40}$$

3. Determine the optimal step length $\rho^{(i)}$:

$$\rho^{(i)} = \text{argmin} J(\boldsymbol{\zeta}^{t(i)} + \rho^{(i)}\mathbf{d}^{(i)}). \tag{41}$$

4. Set

$$\boldsymbol{\zeta}^{t(i+1)} = \boldsymbol{\zeta}^{t(i)} + \rho^{(i)}\mathbf{d}^{(i)}. \tag{42}$$

5. Repeat the above procedure until converged value of $\boldsymbol{\zeta}^t$ is obtained.

The estimated zeta potential along the upper wall is then given by

$$\zeta^t(X) = \sum_{p=1}^{Mx} \zeta_p^t b_p(X). \tag{43}$$

In the conjugate gradient iteration, we have to solve the governing equations repeatedly. Adoption of the reduced-order model instead of the original partial differential equations greatly reduces the computation time.

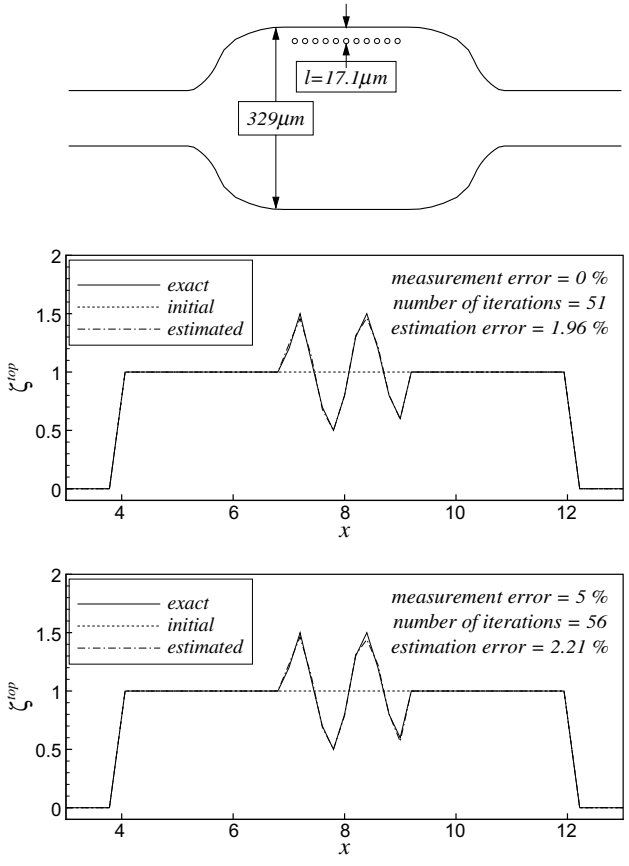

Fig. 8a. Accuracy of the estimation of inhomogeneous zeta potential shape a using the reduced-order model.

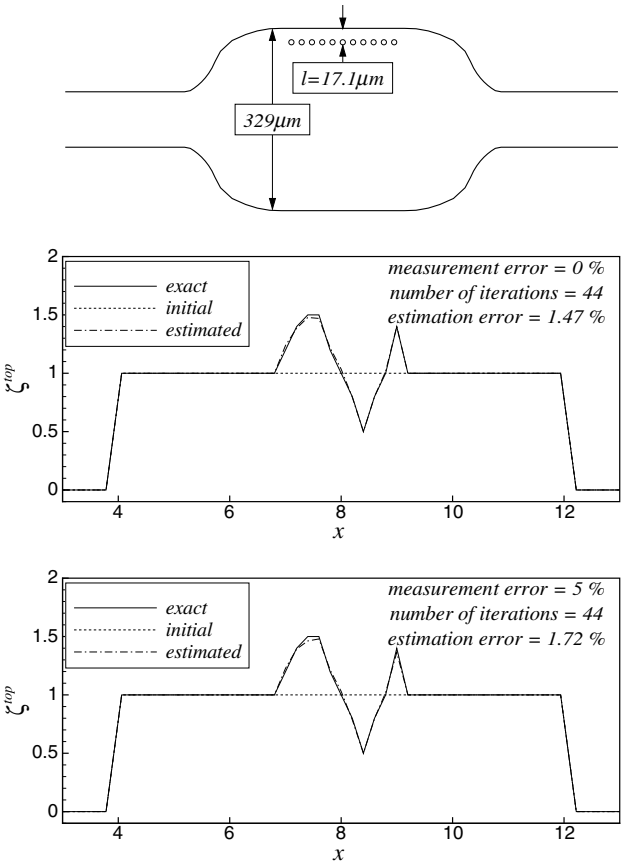

Fig. 8b. Estimation of inhomogeneous zeta potential of shape b.

Fig. 8a and b shows the results of estimation of inhomogeneous zeta potential using the reduced-order model for two different arbitrary profiles. In both cases, the number of measurement locations is 11, each of which is located 17.1 μm away from the wall while the width of the channel is 329 μm. For the case of Fig. 8a, when the initially assumed $\zeta(x)$ is constant (1.0), the conjugate gradient method yields the converged profile after 51 iterations with the estimation error of 1.96% when there is no measurement error and estimation error of 2.21% when the measurement error is 5%. Similarly, for the case of Fig. 8b, the estimation error is 1.47% when the there is no measurement error and the estimation error is 1.72% when the measurement error is 5%. In both cases the conjugate gradient method employing the reduced-order model predicts accurate results, and the estimation error increases with respect to the measurement error.

6. Conclusion

The KLG procedure is employed to reduce the set of partial differential equations governing the electric potential and velocity to a small number of ordinary differential equations. The resulting set of ordinary differential equations, when compared with the original governing equations composed of the Poisson–Boltzmann equation and

the Navier–Stokes equation, could simulate the system almost exactly for arbitrary profiles of zeta potential. Using the reduced-order model, it is attempted to estimate inhomogeneous zeta potential at the upper wall of the microchannel using velocity measurements. The conjugate gradient method employing the reduced-order model is shown to yield accurate estimation even with noisy velocity measurements.

An important as well as interesting consideration in the KLG procedure is the comparison of the CPU time required for the KLG procedure with that for the finite difference method. Unavoidable amount of CPU time is consumed to produce snapshots in the KLG procedure, which must be done by repeated solution of governing partial differential equations for various profiles of zeta potential. Once these snapshots and the resulting empirical eigenfunctions have been secured, the numerical solution of the reduced-order model, Eqs. (25) and (33), for one period of the external potential oscillation (cf. Eq. (29)) consumes only 3.43 s when using the SUN Blade workstation, which should be compared with 919.58 s required in the finite difference solution of the governing partial differential equations employing (80×50) grid system. The reduction in the CPU time is of the order 10^2 in the two-dimensional system as investigated in the present work. The reduction in the CPU time can be estimated a priori since it depends on the number of equations or the number of grid points employed in the numerical analysis. The total number of ordinary differential equations in the reduced-order model is 85, 70 for ψ^h field and 15 for $\mathbf{v}$ field, while the number of grid points in the finite difference method is 4000 for each of ψ, v^x and v^y, a total of 12,000, thus the ratio being a 100th. Therefore, it is expected that the reduction in CPU time for the three-dimensional cases would be of the order of 10^3, since the number of ordinary differential equations of the reduced-order model for the three-dimensional system is almost the same as that of the corresponding two-dimensional system while the number of grids for the three-dimensional system is at least tenfold larger than that for the two-dimensional system. It is hoped that this drastic reduction of CPU time gained by employing the KLG procedure would facilitate the real-time estimation and control of various microfluidic systems.

Acknowledgement

This work was supported by grant no. R01-2003-000-10224-0 from Korea Science and Engineering Foundation.

References

[1] D.J. Harrison, Z.A. Man, Z.A. Fan, H. Widmer, Capillary electrophoresis and sample injection systems integrated on a planar glass chip, Anal. Chem. 64 (1992) 1926–1932.
[2] C.S. Effenhanser, A. Paulus, Z.A. Man, H.M. Widmer, High-speed separation of antisence oligonucleotides on a micromachined capillary electrophoresis device, Anal. Chem. 66 (1994) 2949–2953.
[3] A.E. Herr, J.I. Molho, J.G. Santiago, M.G. Mungal, T.W. Kenny, M.G. Garguilo, Electroosmotic capillary flow with nonuniform zeta potential, Anal. Chem. 72 (2000) 1053–1057.
[4] R.F. Probstein, Physicochemical Hydrodynamics, Wiley, New York, 1994.
[5] H.M. Park, D.H. Cho, The use of the Karhunen–Loève decomposition for the modeling of distributed parameter systems, Chem. Eng. Sci. 51 (1996) 81–98.
[6] H.M. Park, D.H. Cho, Low dimensional modeling of flow reactors, Int. J. Heat Mass Transfer 39 (1996) 3311–3323.
[7] H.M. Park, M.W. Lee, An efficient method of solving the Navier–Stokes equation for the flow control, Int. J. Numer. Meth. Eng. 41 (1998) 1131–1151.
[8] G.P. Books, J.M. Powers, A Karhunen–Loève least-squares technique for optimization of geometry of a blunt body in supersonic flow, J. Comp. Phys. 195 (2004) 387–412.
[9] T. Bewley, R. Temam, M. Ziane, A general framework for robust control in fluid mechanics, Physics D 138 (2000) 360–392.
[10] L. Baramov, O. Tutty, E. Rogers, Robust control of plane Poiseuille flow, AIAA paper no. 2000-2684, AIAA 2000.
[11] H.M. Park, M.C. Sung, J.S. Chung, Stabilization of Rayleigh–Benard convection by means of mode reduction, Proc. R. Soc. Lond. A 460 (2004) 1807–1830.
[12] H.M. Park, M.C. Sung, Stabilization of two-dimensional Rayleigh–Benard convection by means of optimal feedback control, Physics D 186 (2003) 185–204.
[13] A. Kirsch, An Introduction to the Mathematical Theory of Inverse Problems, Springer, New York, 1996.
[14] M. Hanke, Conjugate Gradient Type Methods for Ill-posed Problems, Longman Scientific and Technology, New York, 1995.
[15] M. Loève, Probability Theory, Van Nostrand, Princeton, NJ, 1995.
[16] R. Courant, D. Hilbert, Method of Mathematical Physics 1, Wiley-Interscience, New York, 1962.
[17] P. Moin, R.D. Moser, Characteristic eddy decomposition of turbulence in a channel, J. Fluid Mech. 200 (1989) 471–509.
[18] A.E. Deane, I.G. Kevrekidis, G.E. Karniadakis, S.A. Orszag, Low dimensional models for complex geometry flows: application to grooved channels and circular cylinders, Phys. Fluids 3 (1991) 23–37.
[19] R.J. Hunter, Zeta Potential in Colloid Science: Principles and Applications, Academic Press, 1988.
[20] M.-J. Ni, Projection and simple methods for single-fluid and multiple-fluid incompressible unsteady flows-general formula, Numer. Heat Transf. Part B: Fundamentals 50 (2006) 395–408.
[21] M.M. Rahman, T. Siikonen, An improved simple method on a collocated grid, Numer. Heat Transf. Part B: Fundamentals 38 (2000) 177–201.
[22] Y. Sheng, M. Shoukri, G. Sheng, P. Wood, A modification to the simple method for buoyancy-driven flows, Numer. Heat Transf. Part B: Fundamentals 33 (1998) 65–78.
[23] B. Yu, H. Ozoe, W.-Q. Tao, A modified pressure-correction scheme for the SIMPLER method, MSIMPLER, Numer. Heat Transf. Part B: Fundamentals 39 (2001) 435–449.
[24] K. Shinohara, Y. Sugii, et al., High-speed micro-PIV measurements of transient flow in microfluidic devices, Meas. Sci. Technol. 15 (2004) 1965–1970.